Control of Ocean Temperature on Jakobshavn Isbræ's Present and Future Mass Loss

Johannes H. Bondzio[1] , **Mathieu Morlighem[1]** , **Hélène Seroussi[2]** , **Michael H. Wood[1]** , and **Jérémie Mouginot[1,3]**

[1]Department of Earth System Science, University of California, Irvine, CA, USA, [2]Jet Propulsion Laboratory, California Institute of Technology, Pasadena, CA, USA, [3]Institut des Géosciences de l'Environnement, Grenoble, France

Abstract Large uncertainties in model parameterizations and input data sets make projections of future sea level rise contributions of outlet glaciers challenging. Here we introduce a novel technique for weighing large ensemble model simulations that uses information of key observables. The approach is robust to input errors and yields calibrated means and error estimates of a glacier's mass balance. We apply the technique to Jakobshavn Isbræ, using a model that includes a dynamic calving law, and closely reproduce the observed behavior from 1985 to 2018 by forcing the model with ocean temperatures only. Our calibrated projection suggests that the glacier will continue to retreat and contribute about 5.1 mm to eustatic sea level rise by 2100 under present-day climatic forcing. Our analysis shows that the glacier's future evolution will strongly depend on the ambient oceanic setting.

Plain Language Summary Projections of future sea level rise are important planning information for coastal communities and ecosystems. Large uncertainties in model parameterizations and input data sets make the projections of the contributions of outlet glaciers and ice sheets challenging. Jakobshavn Isbræ in West Greenland is the world's fastest glacier, which retreated for more than 20 km and contributed alone more than 0.1 mm per year to sea level rise after its floating ice tongue broke up at the turn of this millennium. We use a novel technique to calibrate model simulations of Jakobshavn Isbræ using a record of observations in order to (a) understand the causes triggering its recent retreat and (b) produce weighted estimates of the glacier's future contribution to sea level rise. Our analysis shows that the glacier behavior is largely controlled by the oceanic thermal forcing and that its future evolution will strongly depend on the sustained intrusion of warm waters in its fjord. We project that the glacier will contribute an average of 5.1 mm to global sea level rise until 2100 under present-day climatic forcing.

1. Introduction

The Greenland Ice Sheet is the world's second largest ice sheet, with a potential for 7.42 m of eustatic sea level rise (ESLR; Morlighem et al., 2017) and is currently losing mass at an increasing rate (Shepherd et al., 2012). Potential changes in ice flow dynamics remain a major source of uncertainty in ESLR projections (Pachauri et al., 2014), and numerical modeling is the only tool to address this question.

Jakobshavn Isbræ (JI) is the fastest ice stream of the Greenland Ice Sheet and drains about 7% of the ice sheet's surface area. It is responsible, alone, for 4% of the twentieth century sea level rise (Joughin et al., 2004). A sustained intrusion of warm ocean water into its fjord system from 1997 onward likely triggered the disintegration of its ~15-km-long floating ice tongue (Holland et al., 2008), which used to stabilize the glacier (Echelmeyer & Harrison, 1990). Since then, the glacier has rapidly accelerated and has become a major contributor to global sea level rise (Howat et al., 2011; Joughin et al., 2004, 2008, 2014). Currently, the seasonal migration of its calving front triggers widespread acceleration through an interplay of dynamic processes (Bondzio et al., 2017), and it discharges most of its ice through calving. The future evolution of JI remains unclear, and no robust model projections of the evolution of this complex system exist.

Modeling the behavior of marine-terminating outlet glaciers remains challenging. First, several important processes such as calving, submarine melting, and undercutting of the calving front are still poorly understood, despite recent progress (Benn et al., 2017, 2007). Only basic parameterizations of these processes exist, and they may not capture their full complex physics. The sensitivity of an individual glacier to these processes

remains mostly unclear. Second, errors in critical model input data and model parameters, such as the bed topography and oceanic forcing, are largest in regions where they matter most, for example, near the grounding line (Morlighem et al., 2014). It is important to take these uncertainties into account by using an extensive sensitivity analysis or ensemble approach.

In this study, we model the evolution of JI from 1985 to 2100 using a statistical approach. We rely on the Ice Sheet System Model (Larour et al., 2012) to perform a large ensemble of simulations of JI testing through a multidimensional parameter space and compare the model projections to observations of JI over the past three decades (hindcast period). We weigh each simulation with its capacity to reproduce the observed calving front position of JI from 1985 to 2018, which is the primary driver of ice speed change and mass loss (Bondzio et al., 2017). This approach assumes that parameter combinations that produce model glacier behavior closer to observations are more likely to produce realistic projections of glacier behavior and should therefore obtain a higher weight. As a proof of concept, we reproduce JI's observed behavior using this approach and then proceed by producing weighted average estimates of the glaciers mass balance and calving front retreat until 2100. Finally, we discuss the approach and the possible mechanisms responsible for the observed behavior.

2. Model and Experiment Description

2.1. Model Setup

We initialize the model of JI in 1985, which is the earliest year for which a consistent model input data set exists for this glacier. The model domain corresponds to the area of fast ice flow of JI's drainage basin ($|\mathbf{v}| > 100$ m/a; Rignot & Mouginot, 2012). The mesh resolution ranges from 400 m in the trough to 7 km in regions further inland. The resulting two-dimensional mesh has about 13,000 triangular elements.

We derive the ice viscosity parameter from the observed surface temperature lowered by 5 K using the parameterization by Cuffey and Paterson (2010), and we use Glen's flow law with a stress exponent $n = 3$. Basal sliding follows a linear viscous law (Budd et al., 1984). We use the bedrock topography given by BedMachine Greenland version 3 (Morlighem et al., 2017) and a 1985 surface topography derived by photogrammetry (Korsgaard et al., 2016). We fill gaps in the surface topography using data from the Greenland Ice Mapping Project (Howat et al., 2014) corrected with an offset proportional to the ice flow velocity. For all simulations, both hindcast and projections, we use the same constant multidecadal mean surface mass balance taken from RACMO (Ettema et al., 2009).

We rely on a two-dimensional shelfy stream approximation (SSA, MacAyeal, 1989; Morland & Zainuddin, 1987) for the stress balance, as basal sliding is the main contributor to the glacier's fast flow (Lüthi et al., 2002). The grounding line motion is modeled using a subelement migration scheme (Seroussi et al., 2014). We prescribe observed ice flow velocities at the model domain's inflow perimeter and keep the corresponding ice thickness fixed through time.

We use a level set method to simulate the migration of the calving front (Bondzio et al., 2016), which is advected by the difference between the horizontal ice velocity, $\mathbf{v}$, and the sum of the calving rate, c, and the frontal undercutting rate, m_{fr}:

$$\mathbf{w} = \mathbf{v} - \left(c + m_{fr} \right) \mathbf{n},\tag{1}$$

where $\mathbf{n}$ is the outward pointing normal on the calving front.

Calving at JI occurs in the form of both the detachment of large tabular icebergs and the rotating away of smaller blocks of ice from the terminus (Amundson et al., 2010; Echelmeyer & Harrison, 1990). Both processes depend on the presence of sufficient tensile stress to support the fracturing process (Benn et al., 2007). We hence use a modified version of the tensile von-Mises calving rate parameterization from Morlighem et al. (2016) to dynamically evolve the calving front position:

$$c = \|\mathbf{v}\| \frac{\tilde{\sigma}}{\sigma_{\max}}.\tag{2}$$

The parameterization produces calving front retreat once the tensile principal stresses' magnitude at the calving front, $\tilde{\sigma}$, exceeds the stress threshold parameter, $\sigma_{\max}$. Indeed, the stress threshold parameter is the dominant control in this calving law. Numerous physical processes, for example, the density of the ice mélange and the presence of water-filled crevasses, which may influence JI's calving rate (Benn et al., 2007; Cassotto et al., 2015), are not explicitly represented here. Therefore, any seasonal variation in these processes will reflect
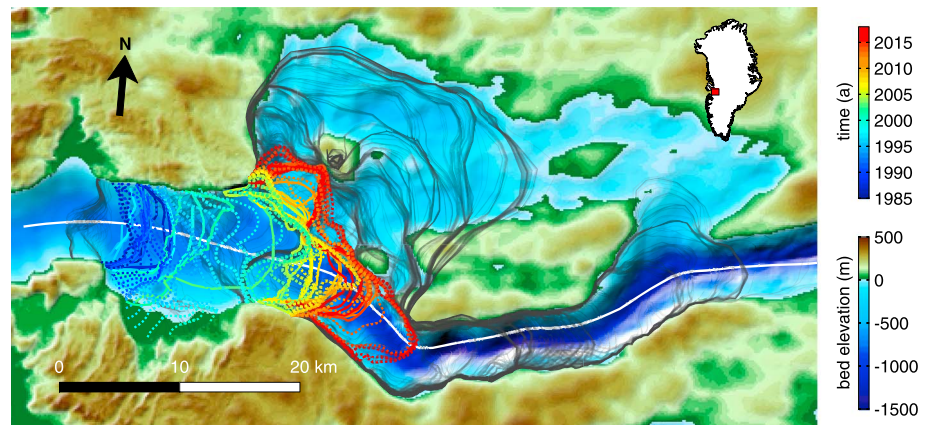
Figure 1. Modeled and observed calving front evolution of Jakobshavn Isbræ until 2018. Colored lines are the calving front positions in summer of each year for a model simulation that obtained a high weight (dotted lines) and observations (continuous lines). Gray lines are the calving front positions for all simulations of the ensemble in summer 2017. The white line is the flow line used for calving front extraction in Figures 3 and 4. Background image: bedrock elevation (shaded relief, BedMachine v3, Morlighem et al., 2017).

in the seasonal value of σ_{max}. We model this seasonality by prescribing $\sigma_{max} = \sigma_{max}(t)$ as a stepwise constant function in time that has a low value each summer (causing retreat) and a high value in winter (causing readvance). The timing of the transitions between summer and winter values is chosen as the average onset of observed calving front advance and retreat: early April and early October each year, respectively. Additionally, observations suggest that the rotation of ice blocks during calving requires a certain minimum height above floatation of the terminus (Joughin et al., 2012). We therefore do not allow calving to occur when the water column between ice base and bedrock measures less than 20 m.

Oceanic forcings such as frontal undercutting of the vertical ice cliff and submarine melting under the ice tongue strongly depend on the ambient fjord water temperature. JI's fjord is choked with icebergs, which renders measurements of fjord water properties difficult. Such measurements are, however, necessary for simulations of the ocean circulation in the fjord, so that we have to rely on simple parameterizations of oceanic forcing instead.

We exploit the observations that (a) the fjord water is typically replaced on subseasonal time scales and (b) the fjord water column is stratified so that its maximum water temperature at depth is the one of the warmest ocean water that is able to spill over the shallow sill at the mouth of the fjord at any time (Gladish et al., 2015). Therefore, we derive depth-averaged fjord water temperatures from the water temperature in the Egedesminde Dyb in the coupled ocean and sea ice simulation provided by the Estimating the Circulation and Climate of the Ocean, Phase II (ECCO2, Menemenlis et al., 2008) project. The depth average is taken between the water surface ($z = 0$) and the maximum of both the fjord sill height ($z = -250$ m) and the local bedrock height. The ECCO2 time series starts in 1992, prior to which we repeat the signal from 1992 to 1996 two times in order to close the data gap between 1986 and 1992 (Figure 3a). In order to prevent immediate calving front retreat due to high submarine melting, we lower the average ECCO2 water temperature, TF, by 2 K until 1996, which is consistent with observations (Holland et al., 2008; Motyka et al., 2011). To extend the forcing to 2100, we repeat this temperature time series from 1985 to 2016 without any change, that is, we prescribe no any additional warming in ocean temperature (Figure 4a).

We use the water temperature time series to compute both the frontal undercutting rates at the calving front, m_{fr}, and the submarine melting rate, m_{sub}. The frontal undercutting rate is computed using the parameterization from Rignot et al. (2016)

$$m_{fr} = \left(A\, h\, q_{sg}^{\alpha} + B \right) TF^{\beta}. \tag{3}$$

Here we set the subglacial discharge, q_{sg}, as the total runoff of JI's drainage basin given by RACMO 2.3 (Noël et al., 2015). We apply frontal undercutting at the terminus only at locations where the water column between ice base and bedrock measures less than 20 m. Hence, calving front retreat in the model is driven either by tensile calving or frontal undercutting. Given that α is small, the effect of q_{sg} is negligible in our simulations.
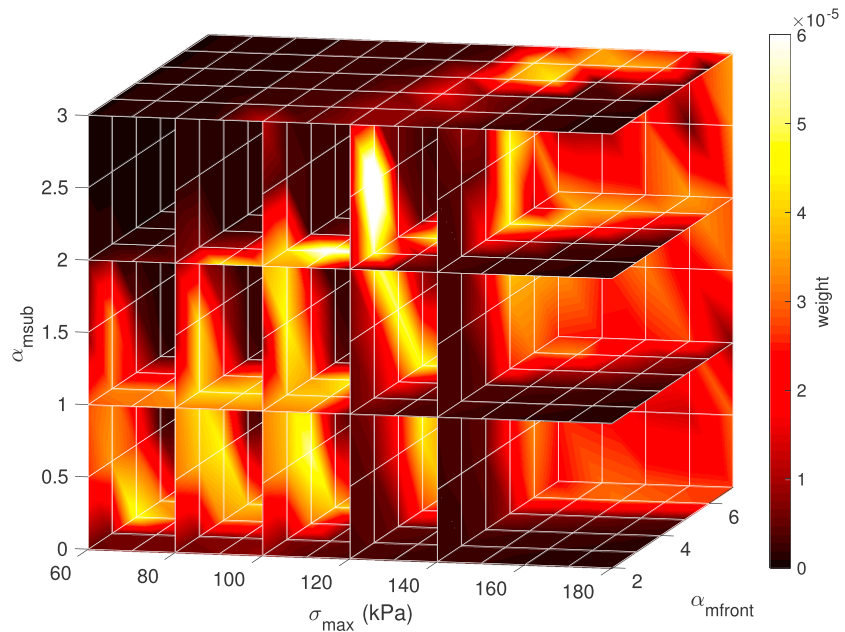
Figure 2. Weights obtained as a function of the parameter combination.

We compute the submarine melting rate using the parameterization from Holland and Jenkins (1999):

$$m_{\text{sub}} = -\rho_M c_{pM} \gamma_T \left(TF - T_{\text{pmp}} \right). \tag{4}$$

Here ρ_M is the ocean layer density, c_{pM} is the specific heat capacity of the mixed layer, γ_T is the thermal exchange velocity, and T_{pmp} is the pressure melting point temperature at the base of the ice shelf.

2.2. Experiments

In this study, we aim to provide an estimate of JI's contribution to future sea level rise until 2100 under present-day climatic forcing. We account for uncertainties related to the internal glacier dynamics and the external forcings from the ocean by performing a large ensemble of simulations, which tests through the different dimensions of a parameter space. As the calving front position is the dominant control on JI's ice flow (Bondzio et al., 2017), our parameter space consists of those parameters relevant to the calving front migration of JI (equation (1)): the stress threshold parameter, σ_{max}, the frontal undercutting rate (applied at the vertical calving face), m_{fr}, and the submarine melting rate (applied under the floating ice), m_{sub}. We do not test the atmospheric forcings as they have been shown to have little impact on ice dynamics on decadal time scales (Seroussi et al., 2013); atmospheric forcings therefore only impact the ice sheet through its influence on ocean conditions and on σ_{max}, respectively.

We use a summer value of σ_{max} ranging from 60 to 180 kPa in steps of 10 kPa across different experiments. The winter value of σ_{max} is 4 MPa in all simulations in order to prevent calving. We scale the frontal undercutting rate with a scaling factor α_{fr} ranging from 2 to 7 in increments of 1. Finally, we scale the submarine melting rate with a factor, α_{sub}, from 0 to 3 in increments of 0.5. This yields a total of 556 parameter combinations. For each parameter combination, we simulate JI's evolution from 1985 to 2100, and the model evolves freely in response to the atmospheric and oceanic forcing.

2.3. Weighing Procedure

We weigh each simulation according to its capacity to reproduce the observed calving front evolution in three steps. First, we compute a distance measure, d, of the modeled calving front position at 1 July of each year, Γ_{mod}, to the observed calving front position that is closest in time, Γ_{obs}. We choose this summer date because of data availability and because the glacier's evolution is controlled to a large degree by its retreat in summer. Including additional annual weighing points does not improve the weight quality substantially. We define d as the largest minimal distance between any two points of the fronts

$$d(\Gamma_{\text{mod}}, \Gamma_{\text{obs}}) = \max_{s \in \Gamma_{\text{mod}}} \min_{r \in \Gamma_{\text{obs}}} |s - r|. \tag{5}$$
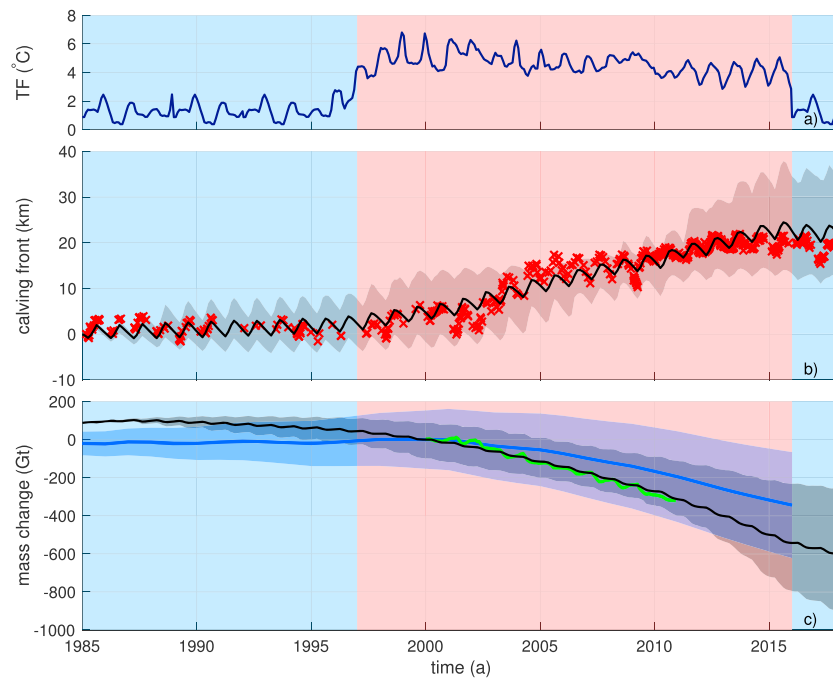
Figure 3. Comparison of average model results and observations. (a) Depth average ocean temperature of Estimating the Circulation and Climate of the Ocean, Phase II in Egedesminde Dyb between 0- and 250-m depths used to force the model. (b) Evolution of the calving front position along the flow line shown in Figure 1. Red crosses show observations. The origin of the y axis is the initial calving front position in 1985. (c) Jakobshavn Isbræ's mass balance. The blue line and shaded error are the mass balance derived from available data products of surface mass balance (RACMO2.3 Noël et al., 2015), ice speed (Mouginot et al., 2017), and ice thickness data (Howat et al., 2014; Krabill & Thomas, 2010; Korsgaard et al., 2016; Morlighem et al., 2014; Zwally et al., 2014). The green line is the estimate given in Howat et al. (2011). The black continuous lines in (b) and (c) are the mean ensemble model outcome of each respective variable, and the gray-shaded area is the corresponding interval between the first and third quartiles. Blue and red shadings in the background mark periods of cold and warm ocean forcing, respectively.

We choose this distance measure as it is sensitive to large retreat along narrow fjords. Second, we assign a *front quality value* to each modeled calving front position as the value of a normal distribution, $N(d, \mu, \sigma)$, with mean $\mu = 0$ km and standard deviation $\sigma = 2$ km of the computed distance measure d. Third, we set the weight, ω, assigned to a model simulation as the time average from 1985 to 2017 of all front quality values

$$\omega = \frac{1}{m} \sum_{i=1}^{m} N(d(\Gamma_{\text{mod}}(t_i), \Gamma_{\text{obs}}(t_i)), \mu, \sigma). \tag{6}$$

Finally, we use the weights to compute weighted means and error estimates of various variables of interest. In the remainder of this paper, *average* and *error estimate* refer to the weighted values of the respective quantity of interest.

3. Results

3.1. Hindcasting and Parameter Calibration

The observed glacier behavior lies well within the range of modeled glacier behaviors produced by the different parameter combinations (Figure 1). The calving law used here reproduces the characteristic calving front shapes of retreating and advancing calving fronts. Generally, the bedrock topography controls the strength of retreat, while the individual parameter combination paired with the oceanic forcing determines the timing and rate of retreat. Due to their different geometrical setting, the two branches of JI react differently to the oceanic forcing. The main, southern branch's calving front, is more sensitive to submarine melting, as it is located in a deep trough, so that submarine melting rates at its grounding line are maximal. The retrograde bed of the trough upstream of today's calving front position favors rapid grounding line retreat through the marine ice sheet instability (Schoof, 2007; Weertman, 1974). This creates a positive feedback between the thinned ice tongue, which calves more easily, and further grounding line retreat through accelerated ice flow.
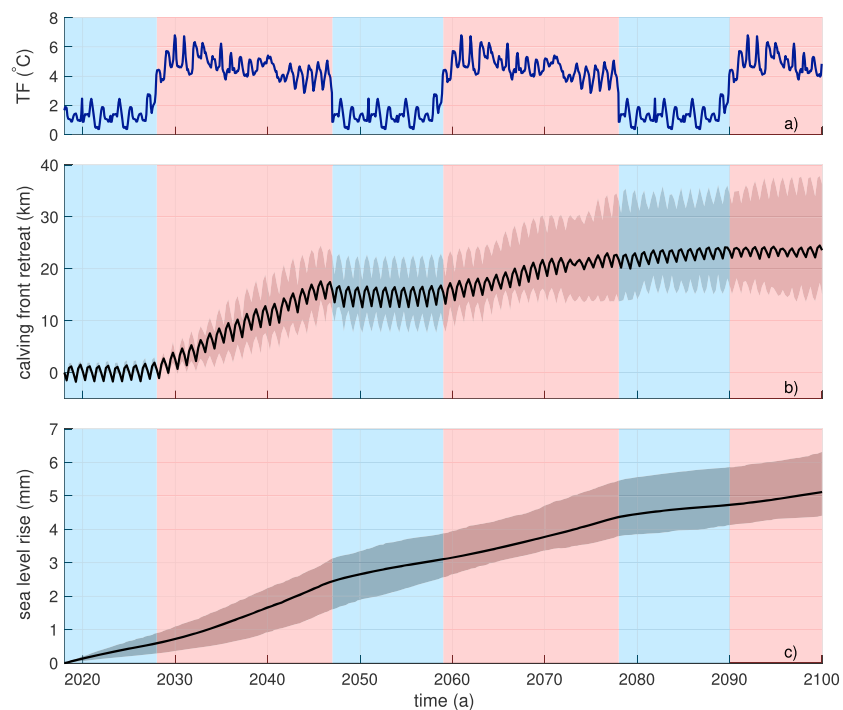
Figure 4. (a) Extended timeline of depth average ocean temperature used to force the model. (b) Timeline of JI's calving front retreat along the flow line shown in Figure 1. (c) Timeline of JI's average future contribution to ESLR. The black lines in (b) and (c) are the average respective value, and the gray-shaded area denotes the interval between the first and third quartiles. Blue and red shadings in the background mark periods of cold and warm ocean forcing, respectively.

Fastest retreat hence occurs through wide and overdeepened sections of the bedrock, as mass flux and tensile stresses peak there. Conversely, the calving front stabilizes at constrictions to ice flow such as bumps in the bedrock or narrow sections of the trough. This leads to a general pattern of intermittent rapid calving front retreat from one stabilization point to the next, and all models tend to stabilize their calving front at the same locations. The strong warming of the ocean past 1997 hence triggers rapid calving front retreat in most models. Once JI's floating ice tongue has disintegrated, the northern branch is more sensitive to frontal undercutting, as the underlying bedrock is shallow and submarine melting rates are lower. Here the feedback between grounding line retreat and increased calving does not unfold, and the warming of the ocean in the 1990s does not cause substantial retreat.

Multiple parameter combinations reproduce the observed calving front sbehavior to a good degree and hence obtain a high weight (Figure 2). High weights are found on a narrow, upward sloping band in parameter space and rapidly drop close to zero outside of it. The distribution of the band is explained by our choice of calving law: higher values for σ_{max} need to be balanced by higher values of α_{fr} and α_{sub} in order to achieve the same calving front behavior. The first two quantities have the same role in the model (equation (1)). Additional submarine melting thins and steepens the ice tongue, so that the stress threshold parameter is more easily exceeded. The highest weights are found on the plane of $\sigma_{max} = 120$ kPa. Our choice of parameter combinations is based on the current knowledge of calving processes and covers the region of the highest weights well.

The average calving front retreat and mass loss from 1985 to 2018 is in excellent agreement with observations (Figure 3). The mean calving front position remains stable at the mouth of the Tissarisoq Ice Bay until the end of the 1990s. The annual variation in calving front position is about 3–4 km. The abrupt warming of the ocean in the late 1990s triggers rapid calving front retreat over the bay, and the calving front gradually retreats to its present-day position. The average mass loss of JI from 2000 to 2018 is 597 Gt. The average rate of mass loss of 33 Gt/a is almost identical to the observations (Howat et al., 2011).

3.2. Forecasting JI's Behavior Until 2100

JI's evolution until 2100 continues to be highly sensitive to the applied oceanic forcing and the bedrock topography in our model (Figure 4). We project that JI's main branch will retreat for another 23.6 km (15.4-3-6.4 km, first to third quartiles) to the head of its overdeepened trough until 2100 (Figure 4b). The calving front retreat is tied to the presence of warm ocean waters and suitable bedrock conditions. The fastest retreat occurs during the next period of sustained ocean warming once the glacier starts to retreat into the overdeepening upstream of the sill the terminus is currently located at. Cooling of the ocean pauses the retreat, at times enabling readvance of up to 2 km. However, a full readvance to its prebreakup position of the early 1990s never occurs due to the large amount of mass the glacier already lost.

JI is likely to contribute a total of 5.1 mm (4.4–6.3 mm, first to third quartiles) to ESLR until 2100 (Figure 4c). The rate of contribution will remain positive throughout the remainder of the century, but its magnitude depends on the ocean temperature and the calving front retreat. Warm periods lead to an increase in mass loss through both enhanced calving, frontal undercutting, and submarine melting, whereas cold periods decrease the mass loss. The average contribution to ESLR in 2100 continues to be substantial at 0.04 mm/a, since the glacier is still adjusting to the retreated calving front position.

4. Discussion

4.1. Ensemble Approach

We present a novel weighing approach for an ensemble of simulations of JI's evolution from 1985 to 2100. The weighted mean of the ensemble closely reproduces JI's observed behavior until 2018 when forced only with ocean temperature. Finally, we present means and error estimates of JI's calving front evolution and mass balance until 2100.

We designed our weighing routine from enhanced understanding of the physical processes that control the evolution of JI, namely, the importance of its calving front position (Bondzio et al., 2017; Joughin et al., 2012; Rosenau et al., 2013). Previous ensemble model studies (Ritz et al., 2015) weigh their ensemble members with respect to the mass balance, a single number that integrates a host of physical processes. We achieve a higher information retrieval in comparison by matching a key control on the glacier's mass balance and dynamics, the calving front position. This yields higher confidence and smaller error bars in, for example, the glacier's projected mass balance. For example, it is conceivable that during the hindcast period an ensemble simulation has a mass balance that is comparable to observations but that exhibits unphysical calving front behavior. This simulation is not likely to produce realistic glacier behavior in the future. The impact of this ensemble member on the projection is virtually eliminated by giving the corresponding parameter combination a low weight.

The ensemble approach applied here is an addition to the existing model studies that couple an Global Climate Model (GCM) and an ice flow model (Fyke et al., 2014; Seroussi et al., 2017). The coupled approach is computationally more expensive and requires high-resolution observations for the calibration of the GCM but in turn provides detailed insight into the processes at the ice-ocean interface. Our approach does not allow for such a detailed process study but is more robust to errors in input data and parameterizations and provides observation-calibrated means and error estimates.

In our models, ocean warming generally translates into increased calving. The additional submarine melting increases the tensile stress at the terminus through thinning and steepening of the ice tongue, which enhances the calving rate. Moreover, the strong dependency of the frontal undercutting rate on the thermal forcing (cf. equation (3)) causes strong retreat once the terminus is close to grounded. Conversely, a cooling of the ocean suppresses calving and frontal undercutting through the inverse processes causing calving front stabilization and eventually, provided sufficient cooling, readvance. Our calving law only includes a subset of processes thought to impact glaciers calving, as no complete physical representation of calving currently exists. However, this simple representation allows to simulate an evolution of JI's calving front that is in good agreement with observations (Holland et al., 2008; Joughin et al., 2004; Sohn et al., 1998). Therefore, the model likely captures the qualitative link between the ocean temperature and calving.

The mechanism between ocean temperature and calving provides an explanation for how a warming ocean was able to trigger the disintegration of the glacier's floating ice tongue in the late 1990s (Holland et al., 2008). Moreover, it supports that the observed ocean cooling in 2016 and 2017 is a significant contributor to the recent observed readvance of the calving front (D. Holland and A. Khazendar, personal communication, 2018).

Despite explaining observations well, we cannot use this model study to exclude that other processes at the ice base and the ice surface have a significant impact on JI's calving. However, we conclude that JI's future evolution will depend strongly on the ambient oceanic setting, and including the ocean component will be critical for reliable mass balance projections.

Comparison of our projections of mass loss until 2100 with the results of other studies shows the importance of including a dynamically evolving calving front in the model. Our mass loss estimate is 5 times the estimate given in Price et al. (2011) and about double of the estimate given in Bondzio et al. (2017). Both studies are comparable in that they prescribe a fixed calving front position until 2100. Our estimate is slightly lower than the range given in Nick et al. (2013), who use a 1-D flow line model with a moving calving front. The offset is due to both the comparatively cooler present-day climatic forcing used here and the impact of lateral glacier stabilization in our model, which tends to delay the calving front retreat by lowering the von-Mises stress through lateral stress transfer to the trough walls.

4.2. Limitations

Several simplifying assumptions were made in our model simulations. First, we use the SSA with no thermal model and a linear viscous basal sliding law (Budd et al., 1984), which may oversimplify the response of the glacier to calving front retreat. However, previous studies have shown that (a) model results of SSA and higher-order flow approximations are comparable (Morlighem et al., 2010), (b) thermal feedbacks in response to calving front retreat at JI cause a short-lived contribution to ice flow of at most 10%, and (c) the basal sliding law applied here is suitable to reproduce JI's behavior to a good degree (Bondzio et al., 2017, both). Therefore, these factors have little impact on century-scale projections given the much larger errors in the input data sets used here (cf. Seroussi et al., 2013). Second, we do neither include local sea level change in the 21st century nor elastic crustal uplift in our model, as these factors will lead to at most meters shift of both coast line and calving front position due to the mostly steep bedrock along JI's trough (Gogineni et al., 2014). Third, the available observational record for calibration originates from a period in which the Atlantic Multidecadal Oscillation shifted from a negative to a positive index. The warming ocean waters triggered widespread glacier retreat along Greenland's coast (Straneo & Heimbach, 2013). The warmer-than-average ocean during most of the model calibration period potentially affects our weighing results. However, since the ocean is expected to warm, we estimate this bias to be small. As we repeat the oceanic forcing of the period 1985–2016 until 2100, our results are not linked to any specific RCP scenario.

Lastly, it is important to note a caveat concerning the weight distribution. Despite our use of established parameterizations for calving, frontal undercutting, and submarine melting, the weight distribution is useable only for a qualitative sensitivity analysis of the glacier to these processes. It shows that the glacier is sensitive to all three processes, but their relative importance may change once other parameterizations are used. This may hold in particular for models that explicitly include time-varying atmospheric forcings. Along a similar line, the parameter space does not necessarily represent physical values. For example, we find the maximum weights on the $\sigma_{max} = 120$ kPa plane, a value about an order of magnitude lower than the reported tensile yield stress of ice (Petrovic, 2003), combined with frontal undercutting rates that are up to 5 times higher than given by its parametrization (equation (3)). This indicates that there is a large degree of uncertainty in the parameterizations used in our study and that a more complex interplay of processes on length and time scales below our model resolution is involved in calving, as suggested by previous studies (e.g., Astrom et al., 2014; Benn et al., 2017).

4.3. Outlook

The ensemble approach used here is applicable to any marine-terminating outlet glacier and hence is suitable to create mass balance projections of entire ice sheets. This will require understanding of the key controls on the evolution of individual glaciers since these do vary (Moon et al., 2014). Future enhanced understanding of the physics of glaciers will contribute to produce better parameterizations of all processes that control the evolution of JI. In particular, new calving laws emerging from high-resolution calving analysis that are better suited for continental-scale ice flow models, as well as enhanced computational resources, are expected to narrow down the error estimates of mass balance projections.

5. Conclusions

In this study, we present a novel method to weigh a large ensemble of simulations with key observations in order to produce calibrated means and error estimates of JI's future evolution. The weighted ensemble is able

to accurately capture JI's observed behavior when driven by oceanic forcing. We project that the glacier will continue to retreat for another 23.6 km (15.4–36.4 km, first to third quartiles) until 2100 under present-day climatic setting, during which it will contribute a total of 5.1 mm (4.4–6.3 mm, first to third quartiles) to eustatic sea level rise. Alternating periods of cold and warm ocean temperatures will continue to cause intermittent calving front stabilization and retreat, respectively. The extent and rates of retreat are also impacted by the glacier geometry. Our results reveal a mechanism that explains why JI's calving front migration, and therefore its dynamics and mass balance, is highly sensitive to ocean temperature. Our study highlights that correct modeling of the ocean component is key for accurate projections of marine-terminating outlet glaciers. The large ensemble approach used here is an addition to complex coupled simulations of GCMs and ice flow models, as it has the benefit of being robust to input data errors and giving weighted means and error estimates. Our approach is applicable to any outlet glacier for which a sufficient observational record exists and thus is suitable to produce calibrated projections of an ice sheet's contribution to eustatic sea level rise.

References

Amundson, J. M., Fahnestock, M., Truffer, M., Brown, J., Lüthi, M. P., & Motyka, R. J. (2010). Ice mélange dynamics and implications for terminus stability, Jakobshavn Isbræ, greenland. *Journal of Geophysical Research*, *115*, F01005. https://doi.org/10.1029/2009JF001405

Astrom, J. A., Vallot, D., Schafer, M., Welty, E. Z., O'Neel, S., Bartholomaus, T. C., et al. (2014). Termini of calving glaciers as self-organized critical systems. *Nature Geoscience*, *7*(12), 874–878. https://doi.org/10.1038/NGEO2290

Benn, D. I., Åström, J., Zwinger, T., Todd, J., Nick, F. M., Cook, S., et al. (2017). Melt-under-cutting and buoyancy-driven calving from tidewater glaciers: New insights from discrete element and continuum model simulations. *Journal of Glaciology*, *63*(240), 691–702.

Benn, D. I., Warren, C. R., & Mottram, R. H. (2007). Calving processes and the dynamics of calving glaciers. *Earth-Science Reviews*, *82*(3-4), 143–179. https://doi.org/10.1016/j.earscirev.2007.02.002

Bondzio, J., Morlighem, M., Seroussi, H., Kleiner, T., Ruckamp, M., Mouginot, J., et al. (2017). The mechanisms behind Jakobshavn Isbræ's acceleration and mass loss: A 3-D thermomechanical model study. *Geophysical Research Letters*, *44*, 6252–6260. https://doi.org/10.1002/2017GL073309

Bondzio, J. H., Seroussi, H., Morlighem, M., Kleiner, T., Rückamp, M., Humbert, A., & Larour, E. (2016). Modelling calving front dynamics using a level-set method: Application to Jakobshavn Isbræ, West Greenland. *The Cryosphere*, *10*(2), 497–510. https://doi.org/10.5194/tc-10-497-2016

Budd, W., Jenssen, D., & Smith, I. (1984). A three-dimensional time-dependent model of the West Antarctic ice-sheet. *Annals of Glaciology*, *5*, 29–36.

Cassotto, R., Fahnestock, M., Amundson, J. M., Truffer, M., & Joughin, I. (2015). Seasonal and interannual variations in ice melange and its impact on terminus stability, Jakobshavn Isbræ, Greenland. *Journal of Glaciology*, *61*(225). 76–88. https://doi.org/10.3189/2015JoG13J235

Cuffey, K., & Paterson, W. S. B. (2010). *The physics of glaciers* (4th ed.). Oxford: Butterworth-Heinemann, Elsevier.

Echelmeyer, K., & Harrison, W. (1990). Jakobshavns Isbræ, West Greenland—Seasonal variations in velocity or lack thereof. *Journal of Glaciology*, *36*(122), 82–88.

Ettema, J., van den Broeke, M. R., van Meijgaard, E., van de Berg, W. J., Bamber, J. L., Box, J. E., & Bales, R. C. (2009). Higher surface mass balance of the Greenland ice sheet revealed by high-resolution climate modeling. *Geophysical Research Letters*, *36*, L12501. https://doi.org/10.1029/2009GL038110

Fyke, J. G., Sacks, W. J., & Lipscomb, W. H. (2014). A technique for generating consistent ice sheet initial conditions for coupled ice sheet/climate models. *Geoscientific Model Development*, *7*(3), 1183–1195. https://doi.org/10.5194/gmd-7-1183-2014

Gladish, C. V., Holland, D. M., Rosing-Asvid, A., Behrens, J. W., & Boje, J. (2015). Oceanic boundary conditions for Jakobshavn glacier. Part I: Variability and renewal of ilulissat icefjord waters, 2001-14. *Journal of Physical Oceanography*, *45*(1), 3–32. https://doi.org/10.1175/JPO-D-14-0044.1

Gogineni, S., Yan, J. B., Paden, J., Leuschen, C., Li, J., Rodriguez-Morales, F., et al. (2014). Bed topography of Jakobshavn Isbrae, Greenland, and Byrd Glacier, Antarctica. *Journal of Glaciology*, *60*(223), 813–833. https://doi.org/10.3189/2014JoG14J129

Holland, D., & Jenkins, A. (1999). Modeling thermodynamic ice-ocean interactions at the base of an ice shelf. *Journal of Physical Oceanography*, *29*(8, Part 1), 1787–1800.

Holland, D., Thomas, R., De Young, B., Ribergaard, M., & Lyberth, B. (2008). Acceleration of Jakobshavn Isbrae triggered by warm subsurface ocean waters. *Nature Geoscience*, *1*(10), 659–664. https://doi.org/10.1038/ngeo316

Howat, I. M., Ahn, Y., Joughin, I., van den Broeke, M. R., Lenaerts, J. T. M., & Smith, B. (2011). Mass balance of Greenland's three largest outlet glaciers, 2000-2010. *Geophysical Research Letters*, *38*, L12501. https://doi.org/10.1029/2011GL047565

Howat, I. M., Negrete, A., & Smith, B. E. (2014). The Greenland Ice Mapping Project (GIMP) land classification and surface elevation datasets. *Cryosphere*, *8*(4), 1509–1518. https://doi.org/10.5194/tc-8-1509-2014

Joughin, I., Abdalati, W., & Fahnestock, M. (2004). Large fluctuations in speed on Greenland's Jakobshavn Isbrae glacier. *Nature*, *432*(7017), 608–610. https://doi.org/10.1038/nature03130

Joughin, I., Das, S. B., King, M. A., Smith, B. E., Howat, I. M., & Moon, T. (2008). Seasonal speedup along the western flank of the Greenland Ice Sheet. *Science*, *320*(5877), 781–783. https://doi.org/10.1126/science.1153288

Joughin, I., Smith, B. E., Howat, I. M., Floricioiu, D., Alley, R. B., Truffer, M., & Fahnestock, M. (2012). Seasonal to decadal scale variations in the surface velocity of Jakobshavn Isbrae, Greenland: Observation and model-based analysis. *Journal of Geophysical Research*, *117*, 1–20. https://doi.org/10.1029/2011JF002110

Joughin, I., Smith, B. E., Shean, D. E., & Floricioiu, D. (2014). Brief communication: Further summer speedup of Jakobshavn Isbræ. *Cryosphere*, *8*(1), 209–214. https://doi.org/10.5194/tc-8-209-2014

Korsgaard, N. J., Nuth, C., Khan, S. A., Kjeldsen, K. K., Bjork, A. A., Schomacker, A., & Kjaer, K. H. (2016). Data descriptor: Digital elevation model and orthophotographs of Greenland based on aerial photographs from 1978-1987. *Scientific Data*, *3*, 160032. https://doi.org/10.1038/sdata.2016.32

Krabill, W., & Thomas, R. (2010). *Icebridge atm l2 Icessn elevation, slope, and roughness*. Boulder, CO: NASA Distrib. Active Archive Center, Nat. Snow Ice Data Center.

Larour, E., Seroussi, H., Morlighem, M., & Rignot, E. (2012). Continental scale, high order, high spatial resolution, ice sheet modeling using the Ice Sheet System Model (ISSM). *Journal of Geophysical Research*, *117*, 1–20. https://doi.org/10.1029/2011JF002140

Lüthi, M., Funk, M., Iken, A., Gogineni, S., & Truffer, M. (2002). Mechanisms of fast flow in Jakobshavn Isbrae, West Greenland: Part III. Measurements of ice deformation, temperature and cross-borehole conductivity in boreholes to the bedrock. *Journal of Glaciology*, *48*(162), 369–385. https://doi.org/10.3189/172756502781831322

MacAyeal, D. R. (1989). Large-scale ice flow over a viscous basal sediment: Theory and application to ice stream B, Antarctica. *Journal of Geophysical Research*, *94*(B4), 4071–4087.

Menemenlis, D., Campin, C., Heimbach, P., Hill, C., Lee, T., Nguyen, M., et al. (2008). ECCO 2: High resolution global ocean and sea ice data synthesis. *Mercator Ocean Quart. Newsl.*, *31*, 13–21.

Moon, T., Joughin, I., Smith, B., van den Broeke, M. R., van de Berg, W. J., Noel, B., & Usher, M. (2014). Distinct patterns of seasonal greenland glacier velocity. *Geophysical Research Letters*, *41*, 7209–7216. https://doi.org/10.1002/2014GL061836

Morland, L., & Zainuddin, R. (1987). Plane and radial ice-shelf flow with prescribed temperature profile. *In Veen, C.J. van der, and Oerlemans, J., eds. Dynamics of the West Antarctica Ice Sheet. Proceedings of a Workshop held in Utrecht, May 6-8, 1985. Dordrecht, D. Rediel Publishing Company*, *117*(40), 117–140.

Morlighem, M., Bondzio, J., Seroussi, H., Rignot, E., Larour, E., Humbert, A., & Rebuffi, S. A. (2016). Modeling of Store Gletscher's calving dynamics, West Greenland, in response to ocean thermal forcing. *Geophysical Research Letters*, *43*, 2659–2666. https://doi.org/10.1002/2016GL067695

Morlighem, M., Rignot, E., Mouginot, J., Seroussi, H., & Larour, E. (2014). Deeply incised submarine glacial valleys beneath the Greenland ice sheet. *Nature Geoscience*, *7*(6), 418–422. https://doi.org/10.1038/ngeo2167

Morlighem, M., Rignot, E., Seroussi, H., Larour, E., Ben Dhia, H., & Aubry, D. (2010). Spatial patterns of basal drag inferred using control methods from a full-stokes and simpler models for Pine Island Glacier, West Antarctica. *Geophysical Research Letters*, *37*, L14502. https://doi.org/10.1029/2010GL043853

Morlighem, M., Williams, C. N., Rignot, E., An, L., Arndt, J. E., Bamber, J. L., et al. (2017). Bedmachine v3: Complete bed topography and ocean bathymetry mapping of Greenland from multibeam echo sounding combined with mass conservation. *Geophysical Research Letters*, *44*, 11,051–11,061. https://doi.org/10.1002/2017GL074954

Motyka, R. J., Truffer, M., Fahnestock, M., Mortensen, J., Rysgaard, S., & Howat, I. (2011). Submarine melting of the 1985 Jakobshavn Isbrae floating tongue and the triggering of the current retreat. *Journal of Geophysical Research*, *116*, 1–17. https://doi.org/10.1029/2009JF001632

Mouginot, J., Rignot, E., Scheuchl, B., & Millan, R. (2017). Comprehensive annual ice sheet velocity mapping using Landsat-8, Sentinel-1, and RADARSAT-2 data. *Remote Sensing*, *9*(4), 364.

Nick, F. M., Vieli, A., Andersen, M. L., Joughin, I., Payne, A., Edwards, T. L., et al. (2013). Future sea-level rise from Greenland's main outlet glaciers in a warming climate. *Nature*, *497*(7448), 235–238. http://www.nature.com/nature/journal/v497/n7448/full/nature12068.html

Noël, B., van de Berg, W. J., van Meijgaard, E., Munneke, P. K., van de Wal, R. S. W., & van den Broeke, M. R. (2015). Evaluation of the updated regional climate model RACMO2.3: Summer snowfall impact on the Greenland ice sheet. *Cryosphere*, *9*(5), 1831–1844. https://doi.org/10.5194/tc-9-1831-2015

Pachauri, R. K., Allen, M. R., Barros, V. R., Broome, J., Cramer, W., Christ, R., et al. (2014). *Climate change 2014: Synthesis report. Contribution of working groups I, II and III to the fifth assessment report of the intergovernmental panel on climate change* (151 pp.). Geneva, Switzerland: IPCC. https://epic.awi.de/37530/

Petrovic, J. (2003). Review mechanical properties of ice and snow. *Journal of Materials Science*, *38*(1), 1–6. https://doi.org/10.1023/A:1021134128038

Price, S., Payne, A., Howat, I., & Smith, B. (2011). Committed sea-level rise for the next century from Greenland ice sheet dynamics during the past decade. *Proceedings of the National Academy of Sciences of the United States of America*, *108*(22), 8978–8983.

Rignot, E., & Mouginot, J. (2012). Ice flow in Greenland for the international polar year 2008-2009. *Geophysical Research Letters*, *39*, L11501. https://doi.org/10.1029/2012GL051634

Rignot, E., Xu, Y., Menemenlis, D., Mouginot, J., Scheuchl, B., Li, X., et al. (2016). Modeling of ocean-induced ice melt rates of five west Greenland glaciers over the past two decades. *Geophysical Research Letters*, *43*, 6374–6382. https://doi.org/10.1002/2016GL068784

Ritz, C., Edwards, T., Durand, G., Payne, A., Peyaud, V., & Hindmarsh, R. (2015). Potential sea-level rise from Antarctic ice-sheet instability constrained by observations. *Nature*, *528*(7580), 115–118. https://doi.org/10.1038/nature16147

Rosenau, R., Schwalbe, E., Maas, H. G., Baessler, M., & Dietrich, R. (2013). Grounding line migration and high-resolution calving dynamics of Jakobshavn Isbrae, west Greenland. *Journal of Geophysical Research: Earth Surface*, *118*, 382–395. https://doi.org/10.1029/2012JF002515

Schoof, C. (2007). Ice sheet grounding line dynamics: Steady states, stability, and hysteresis. *Journal of Geophysical Research*, *112*, 1–19. https://doi.org/10.1029/2006JF000664

Seroussi, H., Morlighem, M., Larour, E., Rignot, E., & Khazendar, A. (2014). Hydrostatic grounding line parameterization in ice sheet models. *Cryosphere*, *8*(6), 2075–2087. https://doi.org/10.5194/tc-8-2075-2014

Seroussi, H., Morlighem, M., Rignot, E., Khazendar, A., Larour, E., & Mouginot, J. (2013). Dependence of century-scale projections of the Greenland ice sheet on its thermal regime. *Journal of Glaciology*, *59*(218), 1024–1034. https://doi.org/10.3189/2013JoG13J054

Seroussi, H., Nakayama, Y., Larour, E., Menemenlis, D., Morlighem, M., Rignot, E., & Khazendar, A. (2017). Continued retreat of Thwaites Glacier, West Antarctica, controlled by bed topography and ocean circulation. *Geophysical Research Letters*, *44*, 6191–6199. https://doi.org/10.1002/2017GL072910

Shepherd, A., Ivins, E., Geruo, A., Barletta, V., Bentley, M., Bettadpur, S., et al. (2012). A reconciled estimate of ice-sheet mass balance. *Science*, *338*(6111), 1183–1189. https://doi.org/10.1126/science.1228102

Sohn, H., Jezek, K., & van der Veen, C. (1998). Jakobshavn glacier, west Greenland: 30 years of spaceborne observations. *Geophysical Research Letters*, *25*(14), 2699–2702. https://doi.org/10.1029/98GL01973

Straneo, F., & Heimbach, P. (2013). North Atlantic warming and the retreat of Greenland's outlet glaciers. *Nature*, *504*, 36–43.

Weertman, J. (1974). Stability of the junction of an ice sheet and an ice shelf. *Journal of Glaciology*, *13*(67), 3–11.

Zwally, H., Schutz, R., & Dimarzio, J. (2014). *GLAS/ICEsat l2 global land surface altimetry data. Version 34. GLAS 14 Product*. Boulder, Colorado: NASA National Snow and Ice Data Center Distributed Active Archive Center.